Epitaxial superconducting tunnel diodes for light detection applications

KRISHNA BALASUBRAMANIAN,[1,2,*] JOHN WRIGHT,[3] ORR ZOHAR,[1] BOAZ TAITLER,[1] SHLOMI BOUSCHER,[1] HUILI GRACE XING,[3,4,5] DEBDEEP JENA,[3,4,5] AND ALEX HAYAT[1]

[1]*Electrical Engineering, Technion – Israel Institute of Technology, Israel*
[2]*Electrical Engineering, Indian Institute of Technology Kanpur, Kanpur 208016, India*
[3]*Materials Science and Engineering, Cornell University, Ithaca, NY 14853, USA*
[4]*Electrical and Computer Engineering, Cornell University, Ithaca, NY 14853, USA*
[5]*Kavli Institute for Nanoscale Science, Cornell University, Ithaca, NY 14853, USA*
[*]krishnab@iitk.ac.in

Abstract: We demonstrate epitaxially integrated nanoscale superconductor tunnel diodes, realized using NbN on GaN thin films. Tuning the growth conditions leads to reduced interface defect density and to the emergence of the superconducting coherence peaks in the interface tunneling characteristics. The degree of disorder in the superconductor is correlated with the variance in the order parameter value of different domains. Epitaxial integration of the nanoscale layers allowed precise control on the quality of the superconductor at the interface, and, by extension, the variance in the order parameter value. The numerical calculations taking a normal distribution of superconducting order parameter at the interface with a fixed variance in its order parameter values closely match the measured interface transport characteristics at different temperatures. Strong sub-gap nonlinearity observed in the differential conductivity measurements were subsequently shown to be sensitive to photon incidence, thereby acting as a photodetector. Usage of superconducting interfaces with semiconducting layers such as GaN permit sensitivity tunability and enable large scale device fabrication and integration.

1.   Introduction

Superconductor tunnel junctions (STJ) have superconducting interfaces with normal materials such as metals [1], insulators such as oxides [2] and semiconductors [3] having multiple applications [4,5,6]. The density of states (DOS) in a superconductor is discontinuous with a gap surrounding the Fermi level [7]. This leads to strong non-linearity in the interface conductivity with a normal material, which is used in electronic signal mixing [6] and wide band sensitive photon/particle detection [5]. Semiconductor based STJs are uniquely suited for applications such as solid-state realization of Majorana fermions [8], superconducting light emitting diodes [9], super-Schottky diode [6], and single photon detection [10]. In addition to sensitive photo detection, STJ also provides 30-fold higher energy resolution than conventional semiconductor-based photodiodes [11]. The number of excess carriers generated in the detector per incident photon varies inversely with the energy gap of detector [12]. A single high energy photon/particle incident on a superconducting detector (conventional, low transition temperature) with a DOS gap of a few meV generate a high density of carriers due to cascading effect, effectively leading to better energy resolution than conventional semiconductor based detectors [5,13]. STJs using semiconductors as the normal material can provide additional capabilities. The semiconductor conductivity can be controlled with dopant density thereby modulating the Schottky barrier and the interface conductivity [7]. In addition, the availability of large area high quality semiconducting substrates is a significant advantage for batch fabrication of device arrays for applications such as photon detector arrays and cameras [11]. However, direct

deposition of superconducting thin films on semiconductors are prone to introduction of disorder, contamination and elemental diffusion from the underlying layers leading to degradation of the superconducting properties [6]. Hence, controllable growth of high-quality superconducting films on conventional semiconductors are critical to realize large scale fabrication of STJ for above mentioned applications [14]. Such steps can bring these scientific novelties closer to commercial applications.

Practical difficulties in realization of STJ using semiconductors lies in controlling surface defect densities on the semiconductor and the disorder introduced in the superconductor during the growth process [15]. Importance of surface electronic states at and near the interface is well recognized and its influence on the Schottky barrier and interface conductivity extensively researched [16]. InAs has been used to interface with superconductors such as Nb, which is the elemental superconductor with highest transition temperature, due to the ability to form very low/non-existent Schottky barrier [17]. In addition to the Schottky barrier, presence of unsaturated dangling bonds, oxides and contaminants dominate charge distribution at the surface strongly affecting the contact resistance. Surface defects, crystallinity of the underlying semiconducting layer and lattice mismatch with the subsequently deposited superconductor strongly determines the disorder in the latter [14]. Disorder in the superconductor lowers the transition temperature and affects the macroscopic order parameter, thereby affecting critical current and magnetic field properties [18]. In addition, disorder also affects the interface conductivity/transparency of the STJ which strongly influences the device characteristics [19,20]. Thus, for practical realization of STJ on semiconductors, in addition to controlling the semiconductor conductivity via doping, it is essential to control semiconductor surface defect density, material crystallinity, as well as disorder in the superconducting thin films.

Here, we demonstrate an epitaxially integrated semiconductor-superconductor tunnel junction. Epitaxial growth of the superconductor on top of the semiconductor enables atomically controlled contact between the two with reduced interface defect density [14]. Sequential deposition of the materials without breaking vacuum also significantly reduces contamination and the formation of oxides, which strongly affects interface conductivity. We further show that temperature control during the superconductor growth phase enables the tunability of the superconductor-semiconductor interface defect density. This combined with proper control of the semiconductor conductivity (via dopant density) allows the precise tailoring of the characteristic conductivity curve for the needs of a particular application. In this report, crystalline NbN thin films are grown epitaxially on GaN films forming pristine semiconductor superconductor junctions. These junctions exhibit a strong non-linearity in the sub-superconducting gap differential conductance. This feature is used here to demonstrate photodetection capabilities with the possibility of photon energy resolution. Additional applications for these devices include sensitive sub-millimeter photon detector in radio astronomy, super-Schottky diode in microwave engineering and video mixing [6].

The GaN and NbN films were deposited in a molecular beam epitaxial system sequentially without breaking vacuum to oxide and contamination free interfaces. The complete stack information is given in Fig. 1(a). First a thick layer (2000nm) of GaN film was grown on top of Sapphire substrates using an AlN transition layer using vapor phase epitaxy technique. A heavily n-doped – to the point of degeneracy ($\sim 1 \times 10^{19}$ cm^3 Si dopants) 200 nm GaN layer was grown on top of the previously grown GaN layer using molecular-beam epitaxy (MBE). The epitaxial NbN$_x$ films were finally grown at 950°C (S$_1$) & 500°C (S$_2$) using a RF plasma assisted MBE system on top of doped GaN thin film. Further details of the NbN growth is provided elsewhere [14]. The crystalline quality of the epitaxially grown films were characterized using X-ray diffraction studies. The result for two different samples used in this work is shown in Fig. 1(b), where peaks corresponding to crystalline GaN [0002] orientation and NbN with [111] orientation can be observed. A root-mean-square surface roughness of less than 1.5 nm, as shown in the inset of

Fig. 1(b), was obtained which was useful for further microfabrication steps. Superconducting properties of the two NbN thin films were characterized using a four-probe resistance measure conducted in a liquid-helium pumped closed-cycle cryostat. A sharp superconducting resistive transition is observed at 13 K for S_1 and at 15 K for S_2, close to typically reported values on RF sputtered thin films [21].
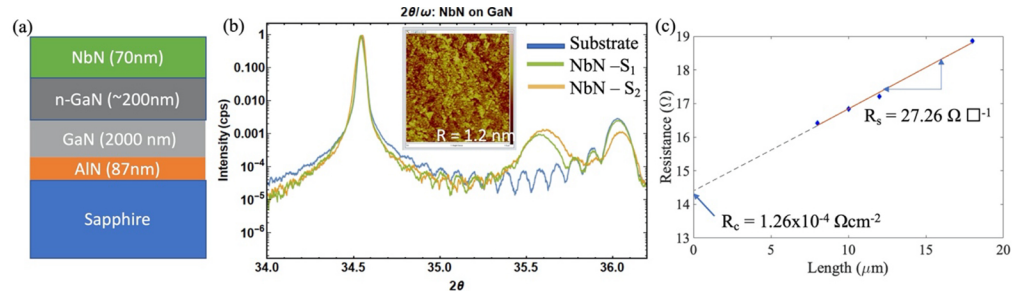

Fig. 1. a) Stack information. b) Symmetric XRD plot showing crystalline GaN and NbN thin films. Surfaces of both the samples were smooth with a roughness of about 1.2 nm. c) Transmission length measurement for contact resistance and sheet resistance extraction at 3 K.

Devices based on STJ between the NbN superconductor and the GaN thin films were formed using standard optical lithographic techniques. The NbN films were etched using a reactive dry etch using SiCl$_4$ plasma. At 40 mTorr pressure and RF power of 150W, the etch rate was found to to be 8–10 nm/min and superconducting pads separated by semiconducting channels with varying lengths were formed. Transmission line measurements (TLM) were conducted on such structures to extract contact resistance of the metallic NbN with the heavily doped N-GaN layer. The results are shown in Fig. 1(c). The calculated sheet resistance of the GaN channel and the contact resistance are also shown. The high n-doping of the topmost GaN layer leads to the observed low sheet resistance. An ohmic contact with low contact resistance is obtained mainly due to the degenerate doping of the GaN layers [22]. This was crucial for realization of usable tunneling transport across the superconductor-semiconductor junctions.

The differential conductance spectra of the junctions were measured from two NbN pads with separations ranging from 2 µm to 20 µm using a lock-in technique. Therefore, the tunneling spectra voltage scale is nearly twice that of a single junction, and the extracted superconducting gap is close to half of the spectral dip in the plots. The lock-in amplifier with a transimpedance amplifier was used in conjunction with a digital multimeter in a four-probe configuration to obtain the conductance measurements. The schematics of the measurement setup is shown in the inset of Fig. 2(a). The differential conductivity extracted from the measurement at various temperatures is shown in Fig. 2(a). The measured conductance of the first sample (termed as S_1) at each temperature was normalized by the normal state conductance measured at 16 K (above the transition temperature of the NbN film). A dip in the normalized conductivity is observed when the bias voltage is below the superconducting order parameter of NbN. This directly follows the shape of the superconducting DOS, where an energy gap corresponding to the temperature dependent order parameter exists. A strongly non-linear sub-gap conductance is observed which is characteristic of superconductor-normal material interface conductance [6].

The differential conductivity follows the DOS of the superconductor [7] and as previously mentioned, should have peaks (coherent peaks) when the voltage bias is close to the twice the order parameter values (for two junctions in series). It can be noted that the conductivity measurement presented in Fig. 2(a) does not show coherence peaks in the conductance. Disorder in the superconductor affects the long-range coherence of the Bardeen-Copper-Schrieffer (BCS)
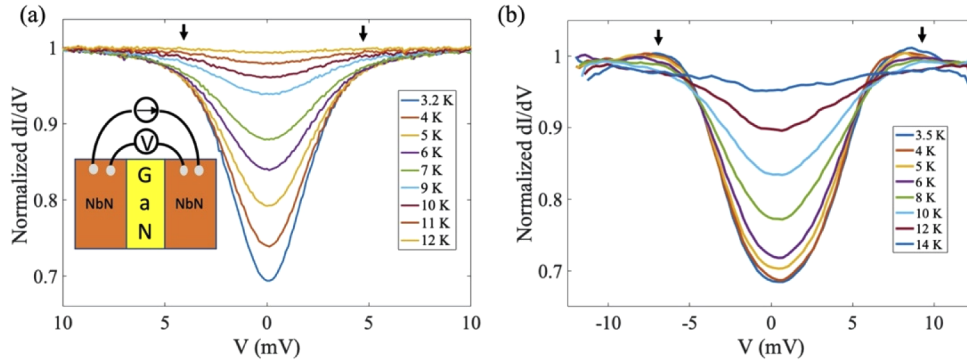
Fig. 2. a) Normalized tunneling conductance of sample S_1 at various temperatures showing a dip in the conductivity sub superconducting gap. Inset shows the measurement schematics. b) Normalized tunneling conductance of sample S_2 with improved interface due to lower growth temperature showing the emergence of coherence peaks. In both the figures, black arrows are indicative of the superconducting gap energies where peaks in conductivity are typically observed.

condensate leading to suppression of the coherent peaks [23,24,25]. Direct deposition of superconductors on normal materials using conventional techniques such as sputtering and evaporation are prone to problems involving surface oxides and contamination leading to uncontrolled interface conductivity. Epitaxial growth enables oxide free integration of materials with excellent crystalline quality [26]. However, even in epitaxial films small degree of disorder is typically introduced due to atomic diffusion from the underlying layers [27], lattice mismatch [28] and thermal expansion mismatch between the two layers. Reducing the growth temperature of the superconducting film drastically reduces atomic diffusion rates and lattice expansion effects. Keeping the other growth parameters, the same, NbN thin films (termed as S_2) were grown at a reduced temperature (500 °C in comparison with the previously mentioned 950 °C). The material quality was monitored using XRD which is shown in Fig. 2(b). The NbN film did not show any significant degradation in the quality as can be seen by the crystalline NbN peaks in the XRD. However, the most important observation came from the superconducting transition measurements and differential conductivity studies. The transition temperature of sample S_2 is higher than S_1 by about 2 K and the emergence of coherence peaks and its variation at various temperatures can be clearly seen in the differential conductivity plots as marked by arrow marks in Figs. 2(a)and 2(b). Observation of such behavior clearly displays the effect of changing the growth condition on the quality of the NbN film.

We now proceed to model the superconductor-semiconductor interface measurements conducted on the two samples to elucidate the effect of interface disorder on transport characteristics. The density of states in the Bardeen-Schieffer-Cooper (BCS) model of superconductor (ρ_s) is given as

$$\rho_S(E) = \begin{cases} 0, & E < \Delta \\ \rho_0 \left(\frac{E}{\sqrt{E^2 - \delta^2}} \right), & otherwise \end{cases} \tag{1}$$

where, ρ_0 is the density of states of the metal at normal state, E is the energy of the particle and Δ is the superconducting order parameter [29]. The current across the interface with a normal material with density of states ρ_N can then be modelled by using [19]

$$I = A \int \rho_N(E) \rho_S(E + eV)(F(E) - F(E + eV)) dE \tag{2}$$

where, V is the applied voltage bias, F is the Fermi Dirac distribution and A is the interface area. The differential conductivity dI/dV can be shown to follow ρ_s when the density of states of the normal material is taken to be almost constant and the Fermi function to be slowing varying around E. Hence in the ideal case, the differential conductivity should have peaks (coherence peaks) at bias voltages close to the order parameter values (Δ). However, practical superconductors, especially thin film materials grown on heterogeneous substrates, typically have disorder [18,25]. Inhomogeneities in the effective interaction between the electrons in the superconductor causes spatial variations in the order-parameter [29]. This leads the superconductor, close to the interface, to have a distribution of order parameter with a spread depending on the degree of disorder. This spread in the order parameter across the superconducting domains reduces the coherence peaks also resulting in increased sub-gap conductance. Numerous experiments with disordered samples have previously been shown to have reduced coherence peaks with varying degrees of increased sub-gap conductance [30].

The averaged DOS in a sample with randomly distributed disorder can be written as [29]

$$\rho(E) = \int_0^\infty \rho(E,\delta) * W\left(\Delta_1, \langle \Delta_1^2 \rangle\right) d\Delta \tag{3}$$

where, W is the distribution function of the order parameter (Δ). Following the original report [29], the Δ was taken to be normally distributed about a mean value of $<\Delta>$ and the distribution is described as

$$W(\Delta) = \frac{1}{\sqrt{2\pi \langle \Delta_1^2 \rangle}} * \exp\left(-\frac{\Delta_1^2}{2 \langle \Delta_1^2 \rangle}\right); \quad \Delta_1 = \Delta - \langle \Delta \rangle, \quad \langle \Delta \rangle = mean(\Delta) \tag{4}$$

Combining the model of averaged DOS with the previously mentioned phenomenological model for interface transport allowed us to accurately model the measured differential conductance of our samples.

The model allows to extract a quantitative value for the deviation in the order parameter between the various superconducting domains, which strongly relates to the degree of disorder in the superconducting material. Additional thermal smearing and finite quasi-particle lifetime effects were introduced via the Dynes parameter (γ) [31]. The numerical calculations to the measured conductivity are given in Figs. 3(a) and 3(b).
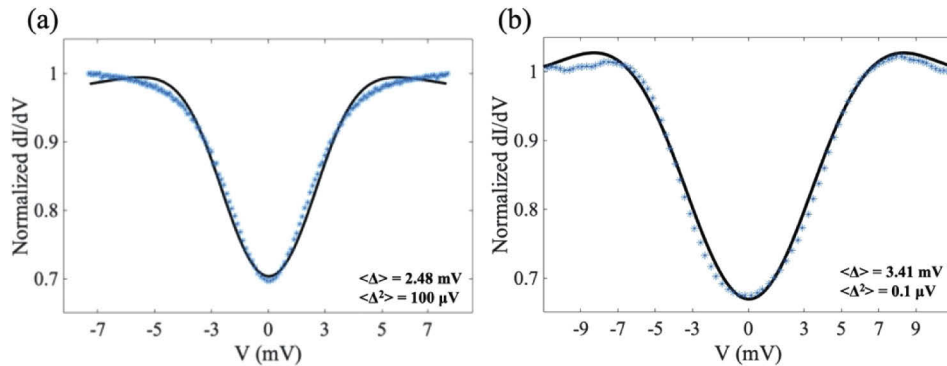

Fig. 3. a) Calculated conductance of sample S_1 showing significantly reduced coherence peaks. b) Conductance of sample S_2 demonstrating emergence of coherence peaks. The corresponding mean and variance in the superconducting order parameter values are also provided.

Reduction in the disorder at the interface of NbN-GaN by changing the deposition conditions resulted in the emergence of a prominent coherence peak as can be noted in Figs. 3(a) and 3(b).

The calculated spread in and the averaged order parameter value for each of the samples are also shown. The superconducting order parameter varies with the transition temperature [7] and the ratio of the calculated effective order parameter value of the two samples match closely with the ratio of transition temperatures [7]. The spread (variance) in the order parameter value (in Figs. 3(a) and 3(b)), which is a qualitative measure of the disorder in the sample, was found to be negligibly small for S_2 and three orders higher for S_1. This model and measurements clearly prove that tuning growth conditions can bring significant improvements in the interface disorder, which includes the emergence of coherence peaks in the superconductor tunneling characteristics.

Small superconducting energy gap, and strong sub-gap non-linearity (Figs. 3(a) and 3(b)) find applications in photon detection. An incident photon breaks a Cooper-pair to create a pair of excited quasi-particles. Since the gap in the superconductor is typically a few meV, and a photon energy is about 2-3 orders higher, excited quasiparticles create a cascade of quasi-particle excitation events. In addition to creation of an effective density of quasi-particles, a portion of the incident photon energy is also lost to the phonon subsystem. Numerical calculations including all the loss processes have been conducted to extract the proportion of photon energy that effectively contribute to excitation of particles. In NbN, the number of quasi-particles per incident photon of energy E_γ were reported to follow the following expression [13]

$$\langle N \rangle = \frac{E_\gamma}{1.7\,\delta} \tag{5}$$

where E_γ is the energy of the incident photon. Photocurrent density due to incident light intensity Φ (Wcm^{-2}) is given by $J = \frac{\eta e \phi}{E_\gamma} \left(\frac{E_\gamma}{1.7\delta} \right)$, where η is the quantum efficiency and e is the electronic charge. The responsivity of the photodetector R_I (A/W), defined as the excess current density in the detector due to unit intensity of the laser incidence. From the enhanced interface conductivity $(\Delta\sigma_I)$ at the bias point due to a light source power density Φ (Wcm^{-2}), R_I can be expressed as

$$R_I = \frac{\eta e}{1.7\delta} \tag{6}$$

The STJ was irradiated with 80 MHz, 5 ps pulsed laser at 800 nm to avoid spurious heating effects from the incident light as shown in Fig. 4. The laser was focussed onto the NbN pad to a spot size of $\sim 5\,\mu m$. The spot was also chosen far away from the interface to avoid spurious interactions with the GaN layers below. The photo induced conductivity under different incident photon densities was measured at 3 K. The resulting plot is shown in Fig. 5(a). While the conductivity sub-gap showed strong laser power dependence (shown by dotted lines) as expected due to the gapped DOS of the superconductor, at bias voltage above the superconducting gap photon incidence does not affect the conductivity due to the excess background quasiparticle conduction. Since, the extinction length of the incident laser in the NbN thin film is estimated to be $\sim$23 nm [32], smaller than the film thickness, the photon interaction is limited to the superconductor alone. This is also evident in vanishing photo-response when biased above the superconducting gap, shown in Fig. 5(a) with a dash-dot line.

The relation between the averaged incident photon density and the change in conductivity is plotted in Fig. 5(b) showing a clear linear dependence. The linear dependence gives an experimental responsivity (R_I) of 0.24 A/W with a dark current of 2 nA, which compares well with the current state of the art avalanche photo diodes [33]. The quantum efficiency of our bare bone device could be further improved by using absorption layers and surface treatments to improve device performance. The detection sensitivity could be in principle enhanced to single photon regime by measuring current using a charge sensitive pre-amplifier [34].
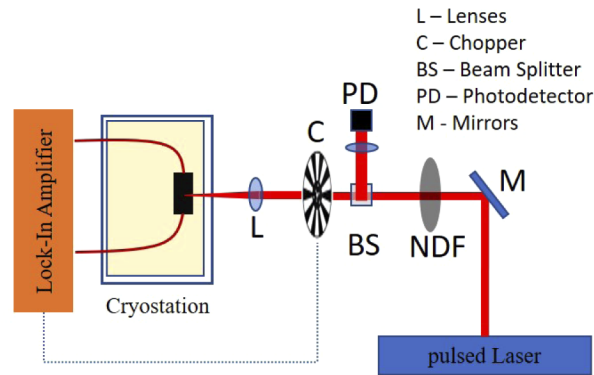
Fig. 4. Schematic representation of the setup for optical measurements. Pulsed laser operating at 80 MHz was used to avoid spurious heating effects and an optical chopper set up was used to modulate the external signal for lock-in detection.
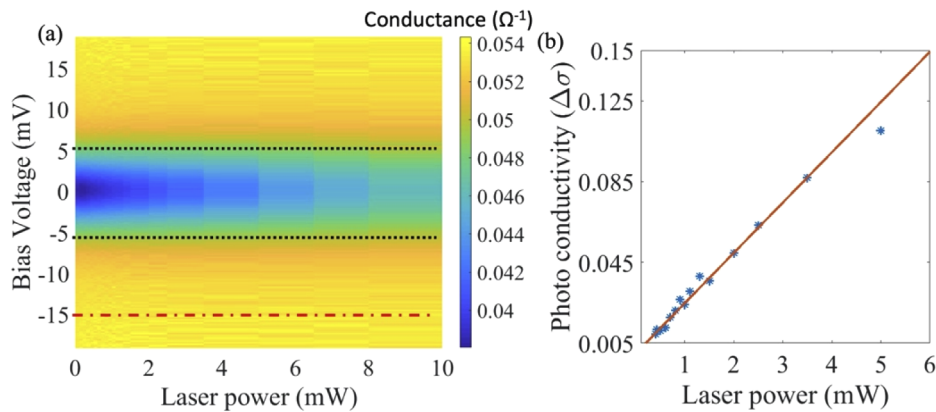

Fig. 5. a) Differential conductivity vs laser power at various bias voltages showing the influence of photon incidence. Dotted line show the superconductor gap edges and the red dash-dot line shows the vanishing photo current at bias voltages above the gap b) Linear fit to the change in the differential conductance at $V_{bias} = 0$ V following Eq. (5).

2. Conclusion

In summary, we show epitaxial integration of superconductors with semiconductors for tunnel diode applications. Using such a precise technique, we demonstrate control on the interface defect density leading to the emergence of coherence peaks in the interface tunneling conductance. A qualitative model for the interface disorder was used to incorporate a variance in the superconducting order parameter at the interface. The extent of this variance was then shown to explain the emergence of coherence peaks as the disorder was decreased. The strong sub-superconducting gap nonlinearity in the interface conductance is shown to demonstrate photon detection capabilities. Demonstration of the capability to epitaxially integrate superconductors on semiconductors not only permit tunable device behavior but also paves the way for large-scale commercial deployment of such devices.

Disclosures

The authors declare no conflict of interest.

References

1. S. D'Ambrosio, M. Meissner, C. Blanc, A. Ronzani, and F. Giazotto, "Normal metal tunnel junction-based superconducting quantum interference proximity transistor," Appl. Phys. Lett. **107**(11), 113110 (2015).
2. D. N. Langenberg, D. J. Scalapino, and B. N. Taylor, "Josephson-type superconducting tunnel junctions as generators of microwave and submillimeter wave radiation," Proc. IEEE **54**(4), 560–575 (1966).
3. T. Akazaki, H. Yamaguchi, J. Nitta, and H. Takayanagi, "Superconductor semiconductor superconductor junctions using NbN," Supercond. Sci. Technol. **12**(11), 901–903 (1999).
4. T. Claeson, "Superconducting Tunnel Junctions in High Frequency Radiation Detectors," in *Advances in Superconductivity* B. Deaver and J. Ruvalds, eds. (Springer US, 1983), pp. 241–277
5. M. Kurakado, "Possibility of high resolution detectors using superconducting tunnel junctions," Nucl. Instrum. Methods Phys. Res. **196**(1), 275–277 (1982).
6. D. Panna, K. Balasubramanian, S. Bouscher, Y. Wang, P. Yu, X. Chen, and A. Hayat, "Nanoscale High-Tc YBCO/GaN Super-Schottky Diode," Sci. Rep. **8**(1), 5597 (2018).
7. M. Tinkham, *Introduction to Superconductivity* (Dover Publications, 1996).
8. J. Cayao, A. M. Black-Schaffer, E. Prada, and R. Aguado, "Andreev spectrum and supercurrents in nanowire-based SNS junctions containing Majorana bound states," Beilstein J. Nanotechnol. **9**, 1339–1357 (2018).
9. D. Panna, S. Bouscher, K. Balasubramanian, V. Perepelook, S. Cohen, D. Ritter, and A. Hayat, "Andreev Reflection in a Superconducting Light-Emitting Diode," Nano Lett. **18**(11), 6764–6769 (2018).
10. A. Peacock, P. Verhoeve, N. Rando, A. Dordrecht, B. G. Taylor, C. Erd, M. A. C. Perryman, R. Venn, J. Howlett, D. J. Goldie, J. Lumley, and M. Wallis, "Single optical photon detection with a superconducting tunnel junction," Nature **381**(6578), 135–137 (1996).
11. S. Friedrich, "Superconducting tunnel junction photon detectors: Theory and applications," J. Low Temp. Phys. **151**(1-2), 277–286 (2008).
12. A. A. Golubov, E. P. Houwman, J. G. Gijsbertsen, J. Flokstra, H. Rogalla, J. B. Le Grand, and P. A. J. Korte, "Quasiparticle lifetimes and tunneling times in a superconductor-insulator-superconductor tunnel junction with spatially inhomogeneous electrodes," Phys. Rev. B **49**(18), 12953–12968 (1994).
13. M. Kurakado, "Developments in superconducting tunnel junction detectors," Nucl. Instrum. Methods Phys. Res., Sect. A **314**(2), 252–262 (1992).
14. R. Yan, G. Khalsa, S. Vishwanath, Y. Han, J. Wright, S. Rouvimov, D. S. Katzer, N. Nepal, B. P. Downey, and D. A. Muller and others, "GaN/NbN epitaxial semiconductor/superconductor heterostructures," Nature **555**(7695), 183–189 (2018).
15. N. A. Güsken, T. Rieger, P. Zellekens, B. Bennemann, E. Neumann, M. I. Lepsa, T. Schäpers, and D. Grützmacher, "MBE growth of Al/InAs and Nb/InAs superconducting hybrid nanowire structures," Nanoscale **9**(43), 16735–16741 (2017).
16. R. H. Williams, "Surface Defects on Semiconductors," Surf. Sci. **132**(1-3), 122–142 (1983).
17. C. Nguyen, H. Kroemer, and E. L. Hu, "Contact resistance of superconductor-semiconductor interfaces: The case of Nb-InAs/AlSb quantum-well structures," Appl. Phys. Lett. **65**(1), 103–105 (1994).
18. J. W. Garland, K. H. Bennemann, and F. M. Mueller, "Effect of Lattice Disorder on the Superconducting Transition Temperature," Phys. Rev. Lett. **21**(18), 1315–1319 (1968).
19. M. Tinkham, "Tunneling generation, relaxation, and tunneling detection of hole-electron imbalance in superconductors," Phys. Rev. B **6**(5), 1747–1756 (1972).
20. M. Tinkham and J. Clarke, "Theory of pair-quasiparticle potential difference in nonequilibrium superconductors," Phys. Rev. Lett. **28**(21), 1366–1369 (1972).
21. K. Buttig, H. Liemersdorf, H. Kinder, and K. Reichelt, "Superconductivity transition temperatures of rf reactively sputtered NbN Films," J. Appl. Phys. **44**(11), 5069–5071 (1973).

22. M. E. Lin, Z. Ma, F. Huang, Z. F. Fan, L. H. Allen, and H. Morkoc, "Low resistance ohmic contacts on wide band-gap GaN," Appl. Phys. Lett. **64**(8), 1003–1005 (1994).

23. K. Bouadim, Y. L. Loh, M. Randeria, and N. Trivedi, "Single-and two-particle energy gaps across the disorder-driven superconductor–insulator transition," Nat. Phys. **7**(11), 884–889 (2011).

24. A. Kamlapure, T. Das, S. C. Ganguli, J. B. Parmar, S. Bhattacharyya, and P. Raychaudhuri, "Emergence of nanoscale inhomogeneity in the superconducting state of a homogeneously disordered conventional superconductor," Sci. Rep. **3**(1), 2979 (2013).

25. S. P. Chockalingam, M. Chand, J. Jesudasan, V. Tripathi, and P. Raychaudhuri, "Evolution of superconducting properties with disorder in epitaxial NbN films," in *Journal of Physics: Conference Series*, (2009).

26. P. Krogstrup, N. L. B. Ziino, W. Chang, S. M. Albrecht, M. H. Madsen, E. Johnson, J. Nygård, C. M. Marcus, and T. S. Jespersen, "Epitaxy of semiconductor–superconductor nanowires," Nat. Mater. **14**(4), 400–406 (2015).

27. T. D. Dzhafarov, "Atomic diffusion in semiconductor epitaxial structures," Phys. Status Solidi A **42**(1), 11–45 (1977).

28. T. Zheleva, K. Jagannadham, and J. Narayan and, "Epitaxial growth in large-lattice-mismatch systems," J. Appl. Phys. **75**(2), 860–871 (1994).

29. A. I. Larkin and Y. N. Ovchinnikov, "Density of States in a Homogeneous Superconductor," Soviet Physics JETP **34**(5), 1144–1150 (1972).

30. M. V. Feigel'man and M. A. Skvortsov, "Universal Broadening of the Bardeen-Cooper-Schrieffer Coherence Peak of Disordered Superconducting Fil," Phys. Rev. Lett. **109**(14), 147002 (2012).

31. R. C. Dynes, V. Narayanamurti, and J. Garno, "Direct Measurement of Quasiparticle-Lifetime Broadening in a Strong-Coupled Superconductor," Phys. Rev. Lett. **41**(21), 1509–1512 (1978).

32. A. Banerjee, R. M. Heath, D. Morozov, D. Hemakumara, U. Nasti, I. Thayne, and R. H. Hadfield, "Optical properties of refractory metal based thin films," Opt. Mater. Express **8**(8), 2072 (2018).

33. J. C. Campbell, "Recent Advances in Avalanche Photodiodes," J. Lightwave Technol. **34**(2), 278–285 (2016).

34. A. Peacock, P. Verhoeve, N. Rando, A. v. Dordrecht, C. E. B. G. Taylor, M. A. C. Perryman, and J. R. Venn, "On the detection of single optical photons with superconducting tunnel junction," J. Appl. Phys. **81**(11), 7641–7646 (1997).